CrossMark

X-Ray and Radio Bursts from the Magnetar 1E 1547.0–5408

G. L. Israel[1] , M. Burgay[2] , N. Rea[3,4] , P. Esposito[5,6] , A. Possenti[2] , S. Dall'Osso[7,8] , L. Stella[1] , M. Pilia[2] ,
A. Tiengo[5,6,9] , A. Ridnaia[10] , A. Y. Lien[11,12] , D. D. Frederiks[10] , and F. Bernardini[1,13,14]
[1] INAF—Osservatorio Astronomico di Roma, via Frascati 33, I-00078 Monteporzio Catone, Italy; gianluca.israel@inaf.it
[2] INAF—Osservatorio Astronomico di Cagliari, Via della Scienza 5, I-09047 Selargius, Italy
[3] Institute of Space Sciences (ICE, CSIC), Campus UAB, Carrer de Can Magrans s/n, E-08193, Barcelona, Spain
[4] Institut d'Estudis Espacials de Catalunya (IEEC), Carrer Gran Capità 2–4, E-08034 Barcelona, Spain
[5] Scuola Universitaria Superiore IUSS Pavia, Palazzo del Broletto, piazza della Vittoria 15, I-27100 Pavia, Italy
[6] INAF—Istituto di Astrofisica Spaziale e Fisica Cosmica di Milano, via A. Corti 12, I-20133 Milano, Italy
[7] Gran Sasso Science Institute, viale F. Crispi 7, I-67100, L'Aquila, Italy
[8] INFN—Laboratori Nazionali del Gran Sasso, I-67100, LAquila, Italy
[9] Istituto Nazionale di Fisica Nucleare (INFN), Sezione di Pavia, via A. Bassi 6, I-27100 Pavia, Italy
[10] Ioffe Institute, 26 Politekhnicheskaya, St. Petersburg, 194021, Russia
[11] Center for Research and Exploration in Space Science and Technology, NASA Goddard Space Flight Center, Greenbelt, MD 20771, USA
[12] Department of Physics, University of Maryland, Baltimore County, 1000 Hilltop Circle, Baltimore, MD 21250, USA
[13] INAF—Osservatorio Astronomico di Capodimonte, Salita Moiariello 16, I-80131 Napoli, Italy
[14] New York University Abu Dhabi, Saadiyat Island, Abu Dhabi, 129188, United Arab Emirates
Received 2020 July 20; revised 2020 October 22; accepted 2020 November 12; published 2021 January 19

Abstract

We report on simultaneous radio and X-ray observations of the radio-emitting magnetar 1E 1547.0–5408 on 2009 January 25 and February 3, with the 64 m Parkes radio telescope and the Chandra and XMM-Newton X-ray observatories. The magnetar was observed in a period of intense X-ray bursting activity and enhanced X-ray emission. We report here on the detection of two radio bursts from 1E 1547.0–5408 reminiscent of fast radio bursts (FRBs). One of the radio bursts was anticipated by $\sim$1 s (about half a rotation period of the pulsar) by a bright SGR-like X-ray burst, resulting in a $F_{\rm radio}/F_{\rm X} \sim 10^{-9}$. Radio pulsations were not detected during the observation showing the FRB-like radio bursts, while they were detected in the previous radio observation. We also found that the two radio bursts are neither aligned with the latter radio pulsations nor with the peak of the X-ray pulse profile (phase shift of $\sim$0.2). Comparing the luminosity of these FRB-like bursts and those reported from SGR 1935 +2154, we find that the wide range in radio efficiency and/or luminosity of magnetar bursts in the Galaxy may bridge the gap between "ordinary" pulsar radio bursts and the extragalactic FRB phenomenon.

Unified Astronomy Thesaurus concepts: X-ray bursts (1814); Magnetars (992); Radio transient sources (2008); Radio bursts (1339); Pulsars (1306); Neutron stars (1108)

1. Introduction

Among the isolated neutron stars, there is a subclass of bright X-ray pulsars believed to be powered by their large magnetic fields, of the order of $\sim 10^{13-15}$ G (see Kaspi & Beloborodov 2017; Esposito et al. 2021 for recent reviews). Among their hallmarks, there are (i) slow rotation periods in the 0.3–12 s range, (ii) X-ray persistent emission modeled by the thermal (0.3–1 keV) emission of a surface hot spot plus a nonthermal magnetospheric component (power law with $\Gamma \sim 2$–4), (iii) emission of X-ray bursts on a wide range of luminosities and timescales ($\approx 10^{38-45}$ erg s^{-1}; ms to minutes), and (iv) large X-ray outbursts lasting years.

The discovery of transient pulsed radio emission following intense X-ray outbursts of five members of the class (Halpern et al. 2005; Camilo et al. 2006; Esposito et al. 2020) was a bolt in the field. The pulsed radio emission from magnetars is characterized by a flat radio spectral index ($S_\nu \propto \nu^{0.5}$) and large variabilities both in flux density and pulse profile (e.g., Camilo et al. 2006; Kramer et al. 2007). To further blur the line between magnetars and "ordinary" pulsars, magnetar-like X-ray activity was found in objects with dipolar B fields as low as 6×10^{12} G (Rea et al. 2010, 2013), and in pulsars with powerful rotational energy loss rate, such as the radio-quiet PSR J1846−0258 (Gavriil et al. 2008) and the radio-loud PSR J1119−6127 (Archibald et al. 2016).

A renewed interest for magnetar radio emission comes from its possible connection to fast radio bursts (FRBs). FRBs are bright ($\sim$ Jy) ms-duration transients whose impulsive nature and extreme brightness temperatures imply coherent emission and connect them to compact objects. When the first repeating FRB was observed (Spitler et al. 2014, 2016) it became clear that at least a selection of FRBs could not be powered by a single explosive event. All these characteristics pointed to a connection with magnetar bursts, possible from very young extra-Galactic magnetars (Beloborodov 2017; Metzger et al. 2017). Recently, the detection of a double-peaked radio burst simultaneous with a bright SGR-like burst from SGR 1935 +2154 (Bochenek et al. 2020; Li et al. 2020; Mereghetti et al. 2020; Ridnaia et al. 2020; The CHIME/FRB Collaboration et al. 2020) showed for the first time that magnetar bursts can indeed have bright radio counterparts.

1E 1547.0–5408 has a $\sim$2.07 s spin period and a surface dipolar magnetic field of $B_{\rm p} \sim 6.4 \times 10^{19}(P\dot{P})^{1/2} \sim 6.4 \times 10^{14}$ G (Dib et al. 2012). Since its discovery (Lamb & Markert 1981; Gelfand & Gaensler 2007), 1E 1547.0–5408 has experienced at least three outbursts (in 2007, 2008, and 2009) during which it emitted several energetic short bursts (Israel et al. 2010; Bernardini et al. 2011; Scholz & Kaspi 2011; Coti Zelati et al. 2020). Multiple expanding X-ray rings were detected around the source during the 2009 outburst decay, allowing an estimate of

Table 1
Main Parameters of the X-Ray and Radio Observations of 1E 1547.0–5408

Date (mm/dd/yy)	Start Time (UT)		Overlap (hr)	T_X/T_{Radio} (hr)	Flux$_X$[a] (erg cm^{-2} s^{-1})	Radio Band		X-Ray P (s)
	Radio	X-Ray				ν (MHz)	$\Delta\nu$ (MHz)	
01/23/2009	23:10:11	⋯	⋯	−/1.17	⋯	3094.0[b]	1024.0[b]	⋯
01/25/2009	16:48:22	15:44:01[c]	1.17	3.37/1.17	$5.74\pm^{0.02}_{0.41}$	2935.5/3094.0[b]	576.0/1024.0[b]	2.07213(2)
02/03/2009	18:28:58	18:23:50[d]	1.51	15.68/1.51	$4.52\pm^{0.01}_{0.04}$	6592.5/6380.5[b]	576.0/256.0[b]	2.072151(2)

Notes.
[a] X-ray flux in units of 10^{-11} and in the 0.5–10 keV energy range. Values are from Bernardini et al. (2011).
[b] DFB observations.
[c] Chandra observation.
[d] XMM-Newton observation.

the source distance of ∼4.5 kpc (Tiengo et al. 2010; in the following, we adopt this distance value).

In this work, we present simultaneous X-ray and radio observations of 1E 1547.0–5408 performed in 2009, while it was undergoing its brightest outburst. A summary of the results and a discussion are presented in Sections 3 and 4.

2. Observations and Analysis

2.1. X-Ray Data Sets

On 2009 January 25, 1E 1547.0–5408 was observed with the S3 CCD of the ACIS camera on board Chandra (Table 1). The observations were performed in Continuos Clocking mode (time resolution of 2.85 ms) and standard data processing and reduction were performed with the CIAO software package (v. 4.10) and the calibration files in CALDB (v. 4.8). We extracted the source events in the 0.3–10 keV energy range from a 3″5 region around the source position (R.A. = 15:50:54.12, decl. = −54:18:24.05, J2000), and the background from a region of the same size.

On 2009 February 3–4, 1E 1547.0–5408 was observed with XMM-Newton with all EPIC cameras operating in Full Frame mode (frame time of 73.4 ms and 2.6 s, for the pn and MOS, respectively). The data were processed and reduced with standard procedures using the SAS software package. The source photons were accumulated from a circular region with radius of 36″, while the background was estimated from a circle of the same size in the same chip as the source. To search for bursts, we extracted the EPIC-pn events from the full detector because bright magnetar bursts can cause heavy pile-up and other saturation effects that substantially reduce the number of valid events at the source position. To study the properties of the persistent emission of the source, the time intervals of the detected bursts (see Figure 1) were excluded from the analysis by applying an intensity filter (with a negligible reduction of the net exposure time; see Table 1).

1E 1547.0–5408 also triggered Konus-Wind (KW; Aptekar et al. 1995) during our simultaneous radio/X-ray campaign on 2009 February 3. KW consists of two identical NaI(Tl) scintillation detectors with a 2π steradians field of view (FoV), operating from 20 keV to 16 MeV. In the triggered mode, activated when the count rate in the 80–320 keV band exceeds a ≈9σ threshold above background, light curves with a time resolution up to 2 ms are recorded in three energy bands, starting from 0.512 s before the trigger time T0.

At the same epoch the Burst Alert Telescope (BAT) on board Swift (Gehrels et al. 2004) also detected a significant count rate increase coincident in time (and shape) with the KW
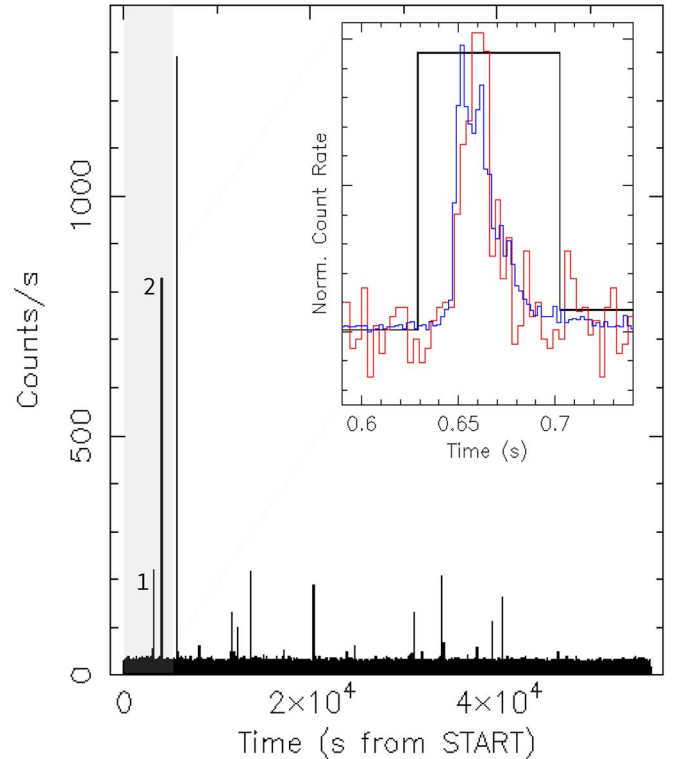

Figure 1. XMM-Newton EPIC-pn 2–10 keV light curve binned at 0.5 s, where the gray area marks the time interval covered by Parkes observations. The detected X-ray bursts within the radio overlap interval are marked as "1" and "2". The inset shows burst "2" as observed by EPIC-pn in the 2–10 keV band (black line; time resolution 73.4 ms), Swift/BAT in the 15–100 keV band (red line; time resolution of 3 ms), and KW in the 20–1400 keV band (blue line; time resolution of 2 ms).

trigger. BAT is a coded-mask instrument operating in the 15–150 keV band with an FoV of about 1.4 steradians (half-coded). At the time of the trigger 1E 1547.0–5408 was outside the BAT FoV, and no source was found in the BAT image. However, high-energy photons can reach the BAT detector from different directions, and even an out-of-FoV source can sometimes cause a count-rate increase in the BAT detectors.[15] No spectral information can be obtained in such cases and only timing information is recorded.

For the timing analysis, the Chandra, XMM-Newton, KW, and Swift photon arrival times were referred to the barycenter of the solar system using the JPL-DE405 ephemeris. The

---

[15] See https://swift.gsfc.nasa.gov/analysis/bat_swguide_v6_3.pdf.

epochs of the bursts discussed in the following are in barycentric dynamical time (TDB).

2.2. Radio Data Sets

We observed 1E 1547.0–5408 with the Parkes 64 m telescope three times during its 2009 outburst: on 2009 January 23 and 25, and on February 3. On January 23 data were recorded at a central frequency of 3.1 GHz with the digital filterbank backend DFB3,[16] over a 1024 MHz bandwidth split into 1 MHz wide channels and were on-line folded with constant period to form 1024 phase bins and 30 s long subintegrations, for a total of 1.2 hr. On January 25, in parallel with the DFB3, we also acquired data with the analog filterbank AFB in search mode, over a total bandwidth of 576 MHz (centered at 2.9 GHz) split in 3 MHz wide channels. AFB data were 1 bit digitized every 1 ms, while DFB3 data were folded on-line with the same parameters and duration as the previous observation, providing total overlap with X-ray data. For the third observation on February 3, we collected data at a central frequency of 6.6 GHz for 1.5 hr beginning at 18:28:58, i.e., about 5 minutes after the start of the X-ray observation. Data were collected simultaneously with the AFB using 3 MHz wide channels covering a total bandwidth of 576 MHz and with the DFB3 using 0.5 MHz wide channels and a total bandwidth of 256 MHz centered at 6.4 GHz. AFB data were 1 bit sampled every 1 ms, while DFB3 data were folded on-line with the same parameters adopted for the previous observations (1024 phase bins, 30 s subintegrations).

3. Results

3.1. X-Ray Results

By means of a phase-coherent timing analysis, we measured a spin period of $P = 2.07213(2)$ s in the Chandra data set, and $P = 2.072151(2)$ s in the XMM-Newton one (1σ confidence level). We checked that these values are in agreement with the long-term phase-coherent timing solution presented in Bernardini et al. (2011). Both the pulse shape and the pulsed fraction (PF, defined as the semi-amplitude of a sinusoidal function divided by the source average count rate) changed significantly between the two X-ray observations: from an almost sinusoidal to a double-peaked pulse profile, and from PF = $10 \pm 1\%$ to $15 \pm 1\%$ (in the 0.5–10 keV interval).

The search for bursts was performed on the 2–10 keV light curve of the full EPIC-pn detector, with a bin time of 0.5 s. We label as a burst every bin with a probability <0.001 of being a Poissonian fluctuation of the average count rate, considering the number of time bins of the light curve as the number of independent trials. Based on this definition, we detected 11 bursts in the XMM-Newton X-ray light curve and only two in the interval covered also by the Parkes observation. The TDB time of the latter two bursts ("1" and "2" in Figure 1) are 19:17:10.5 and 19:31:28.5. The 0.5 s time bin associated with the two bursts contains 90 and 374 pn events, respectively.

During the peak of burst "2," some of the pn quadrants, consisting of three CCDs sharing the same electronics, were fully saturated and registered no valid events, making it impossible to evaluate the burst fluence. On the other hand, burst "2" was detected in a single 2.6 s frame in both the MOS cameras. In this case, the burst is heavily piled-up, with no

events detected in the PSF core, but a reliable spectrum could be extracted from a 2′–5′ annular region, containing 120 and 122 counts in MOS1 and MOS2, respectively, in the 2–10 keV energy range.

Burst "2" was also seen by Swift BAT (TDRSS ObsID 00341964000) even though the source was out of the nominal FoV at the time of the event. No spectral information is available but it provided us with an accurate peak barycentered time of 19:31:28.66 TDB.

Furthermore, burst "2" triggered KW at $T_{0,KW} = 19{:}31{:}28.646$ TDB (with an accuracy of a few milliseconds). The EPIC-pn, BAT, and KW light curves are shown in Figure 1.

Spectral information could be derived from the KW data, from 16 to 80 ms after the rise of the burst. This spectrum contains 400 background-subtracted counts in the 20–300 keV energy band. The light curves in the 20–80 keV and 80–350 keV bands show no evidence of spectral changes along the burst evolution. We therefore performed a joint analysis of the KW and MOS spectra by applying to the model of the KW spectrum a cross-normalization factor accounting for the instrumental dead-time and the fraction of burst background-subtracted counts detected in this 64 ms time interval. We obtained a good fit ($\chi_\nu^2 = 1.6$ for 16 d.o.f.) with a double blackbody model, with photoelectric absorption fixed at $N_H = 4.2 \times 10^{22}$ cm^{-2} (Pintore et al. 2017), obtaining the following best-fit parameters:[17] $kT_1 = 4.1 \pm 0.2$ keV and $R_1 = 65 \pm 4$ km, $kT_2 = 14.3 \pm 0.8$ keV and $R_2 = 5.5 \pm 0.8$ km. From this model, we derive a bolometric fluence of 2.6×10^{-6} erg cm^{-2}. The observed fluence in the 2–10 keV and 20–100 keV is 3.1×10^{-7} erg cm^{-2} and 1.5×10^{-6} erg cm^{-2}, respectively. A much worse fit ($\chi_\nu^2 = 2.2$ for 17 d.o.f.) was obtained by adopting an absorbed cutoff power-law model.

Also burst "1" was detected by the MOS cameras. Due to its lower fluence, we could safely extract its spectrum from an annulus with a smaller inner radius (20″), containing 35 counts in MOS1 and 37 counts in MOS2. Assuming the same best-fit spectral model as burst "2," its fluence in the 2–10 keV energy band is only 4.5×10^{-9} erg cm^{-2}.

3.2. Radio Results

We first searched for radio pulsations during the three Parkes observations. No radio pulsations were detected from 1E 1547.0–5408 in our first observation, taken on January 23, down to a flux density limit of ∼0.06 mJy. The source was again visible as a radio pulsar on January 25 (Burgay et al. 2009). As expected, the rotational ephemeris available in the literature did not satisfactorily phase align the radio data. A local timing solution obtained from the X-ray data (Bernardini et al. 2011) was used to correctly fold off-line the radio data. In the third observation on February 3, no pulsations were detected, but only two single pulses/bursts were observed, at epochs 19:31:29.82 (pulse A) and 19:31:34.05 (pulse B) TDB. The reported times are also corrected for the dispersion delay (using the dispersion measure DM = 830 ± 50 pc cm^{-3}, from Camilo et al. 2007b) at the observing frequency. The error on the DM results in an uncertainty in the bursts arrival times of 4.4 ms. All times are reported at infinite frequency.

---

[16] See http://www.srt.inaf.it/media/uploads/astronomers/dfb.pdf.

[17] To evaluate the blackbody radii, a burst duration of 20 ms was assumed.

Pulse A was so strong to saturate for about 0.2 seconds the AFB backend. This can be clearly seen from the red curve in Figure 3, where pulse A shows a flat top and the baseline following it shows a significant distortion. Pulse B was also likely very close to the saturation level, as can be inferred from the value of its highest point and from the (smaller than for pulse A) distortion of the baseline. For pulse A the time of arrival reported above refers to the mid-point of the saturated portion, while for pulse B it refers to the highest point in the profile.

Taking into account the 1 bit sampling, the 1 ms sampling time, and the frequency width of the channels in use, we can place a lower limit for the flux density necessary to saturate the backend. Using the receiver's system temperature and gain (55 K and 0.71 K Jy^{-1} respectively[18]), we obtain a peak flux density lower limit for the pulse A of $\gtrsim 1$ Jy. Given the 0.2 s duration of the saturation, this corresponds to a lower limit in the pulse fluence of $\gtrsim 200$ Jy ms.

Thanks to the simultaneous observations obtained with the DFB3, we can also give an approximate estimate of the actual peak flux density of the saturated pulse. Even though the data were folded on-line, in fact, the two pulses fall in two separate, consecutive, 30 s long subintegrations. The signal-to-noise ratio of pulse A (averaged with ~15 "silent" rotations) is, in the DFB3 data, three times larger than that of pulse B, also smoothed by the noise resulting from ~15 "silent" rotations. Since pulse B is very close to saturating the AFB, we can tentatively conclude that pulse A must be approximately three times stronger than the saturation limit for the AFB. We can hence estimate a fluence of ~0.6 kJy ms.

To align in phase the X-ray and radio observations of the bursts, we first measured the times of arrival (ToAs) of a fiducial point of the radio profiles (the peak or, in the case of the saturated pulse, the mid-point of the saturation plateau). For the two single pulses the times were obtained directly from the time series, then barycentered and corrected for the dispersion delay at the observed radio frequency using PREPDATA, from the PRESTO package.[19] On the other hand, the ToA of the peak of the folded profile of the pulsations observed on January 25 was measured by cross-correlation with a synthetic profile template using PAT from the PSRCHIVE package (van Straten et al. 2012), and then barycentered and corrected for the dispersion delay using the GENERAL2 plugin in TEMPO2[20] (Hobbs et al. 2006). A local set of ephemerides obtained from the simultaneous X-ray observations was used in the process. The same ephemerides were used to determine the fractional part of the absolute phase of the radio pulses, from which we obtained the phase offset between the selected bin in the radio profiles and the beginning of the first bin of the X-ray light curve.

The results are shown in Figures 2 and 3 where the total X-ray folded light curve is almost aligned with the radio pulses. This result is at variance with that obtained by Halpern et al. (2008), who found ~0.2 cycles phase shift between the X-ray and radio profiles (with the X-rays peak preceding the radio one). This is not surprising because the source is known to vary its profile shape and hence also the exact position of its main peak (Camilo et al. 2007b; Bernardini et al. 2011). Moreover, the single pulses (even for otherwise ordinary pulsars) are often
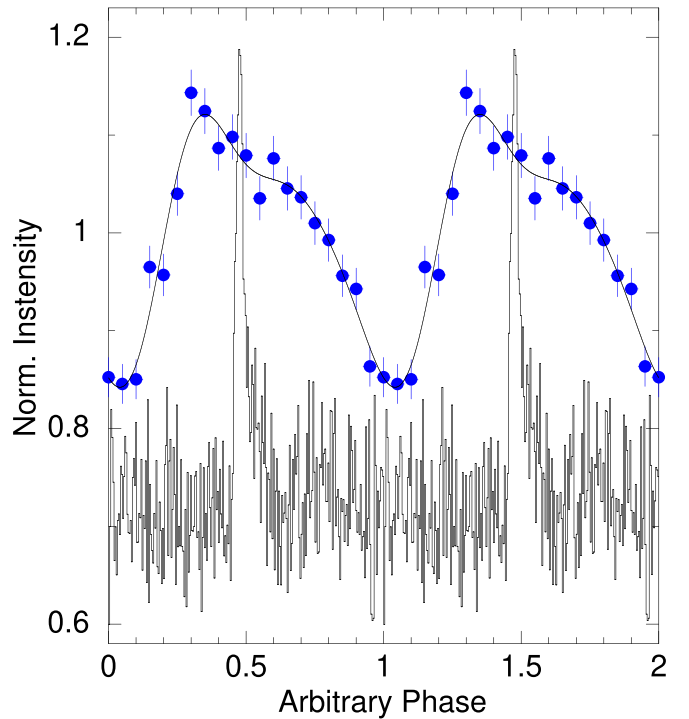
Figure 2. X-ray and radio pulse profiles of 1E 1547.0–5408 from the Chandra ACIS-S (0.5–10 keV) and 3.1 GHz Parkes light curves obtained on 2009 January 25. Superimposed to the X-ray folded light curve is the best fit obtained with the sum of sinusoidal functions.

seen to wander around the integrated peak profile with notable exceptions (as an example the case of XTE J1810-197; Camilo et al. 2007a).

3.3. Radio/X Chance Coincidence Probability

We estimated the probability of having two radio pulses occurring by chance within ~1.2 s (about half a rotation cycle) of the two X-ray bursts detected in the window of radio/X-ray simultaneity on February 3. The 0.5 s bin time of the X-ray light curve corresponds to the zero height width of the saturated radio pulse and yields to $\mathcal{N} \approx 10{,}800$ bins in the time interval of interest. As a conservative approximation, we assume the probability of chance coincidence as the ratio between N_c, the total number of configurations in which one random radio pulse may follow one X-ray burst by $\leqslant 3$ bins, and $\mathcal{N}$, the total number of bins. We obtain $N_c = 12$ as the number of trials (2 radio pulses) times the number of targets (2 X-ray bursts) times the number of valid bins per trial (3), which implies a (maximum) chance coincidence probability of 1.1×10^{-3} (3.3σ). Similarly, we obtain a probability of 7.3×10^{-4} (3.5σ) by considering the two-bin delay ($\lesssim 1$ s) between the X-ray burst peak and the start of the radio pulse.

4. Discussion

We performed two X-ray and three radio observations of 1E 1547.0–5408 during its 2009 burst active phase. In our 1.5 hr long 2009 February 3 observing campaign we detected two bright radio pulses/bursts. In particular, the first event (pulse A), with fluence $F \sim 0.6$ kJy ms and width ~200 ms, occurred about 1 s (half a rotation cycle) after a very bright X-ray burst (burst "2") showing a profile with two peaks separated by 10 ms. The X-ray burst had a bolometric fluence
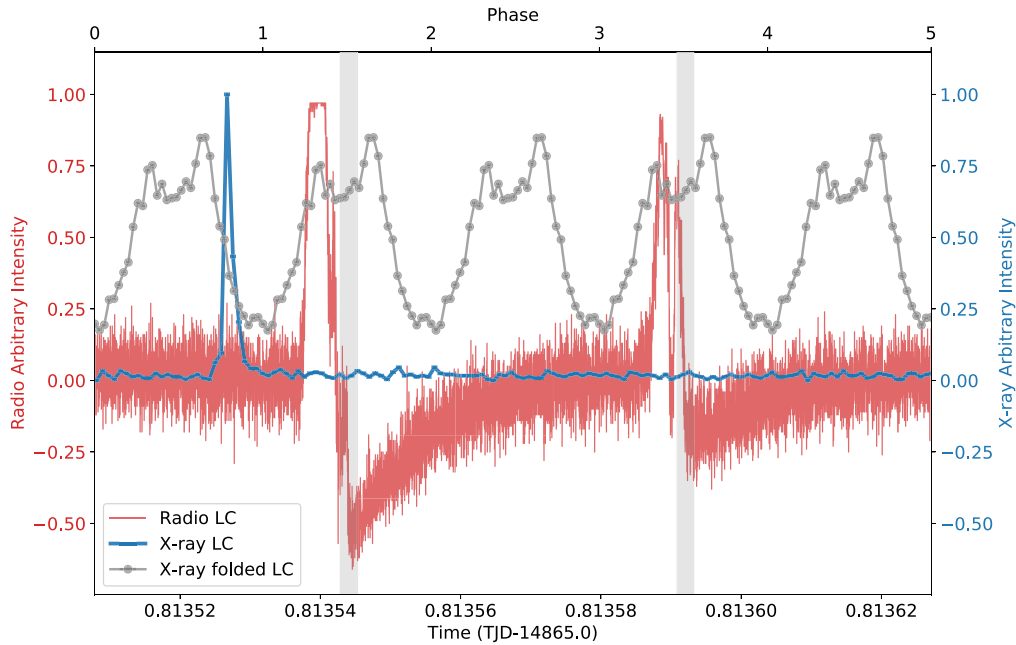
Figure 3. X-ray and radio simultaneous observations of 1E 1547.0–5408 performed on 2009 February 3, around the time of the brightest X-ray burst (burst "2" in Figure 1) and the two radio pulses (pulse A and B). The blue line is the burst light curve, while the gray line is the X-ray folded light curve using the XMM-Newton data set. The Parkes simultaneous radio light curve is shown in red. The gray shaded areas are the phase intervals of the expected peak of the radio pulse profiles extrapolated from the 2009 January 25 Parkes observation (see also Figure 2). Note that the flat top of the first radio peak (pulse A), and the drop of the intensity of the radio signal below the average noise level following both pulses, are artifacts caused by the saturation of the backend.

of 1.3×10^{-6} erg cm^{-2} and width of ~ 50 ms. The radio bursts are neither aligned with the radio pulsations detected six days before in a previous radio observation, nor with the X-ray pulsations, presenting a ~ 0.2 phase shift with respect to both. These findings, along with the lack of "normal" radio pulsations during our 1.5 hr long observation, strongly suggest a close connection of the X-ray and radio bursts. This new and peculiar magnetar phenomenology assumes additional relevance in the context of the recently detected FRB-like bursts from SGR J1935+2154 (Bochenek et al. 2020; Li et al. 2020; Mereghetti et al. 2020; Ridnaia et al. 2020; Tavani et al. 2020; The CHIME/FRB Collaboration et al. 2020). Two bright radio bursts were detected from SGR J1935+2154, with a total fluence of ~ 700 kJy ms at 600 MHz. The second of them was also independently observed by STARE2 at 1.5 GHz, with an estimated fluence above 1.5 MJy ms (Bochenek et al. 2020). Furthermore, the reported radio bursts show a steep spectral index, as do FRBs. In our case, the spectral properties of the radio bursts cannot be constrained as we only observed at 6.6 GHz.

In the case of SGR J1935+2154, despite a slight misalignment of the X-ray peaks as observed by different instruments (Li et al. 2020; Mereghetti et al. 2020; Ridnaia et al. 2020), the radio burst appears to lead the SGR-like X-ray burst by no more than ~ 8 ms, while in 1E 1547.0–5408 it is the X-ray burst that leads the first radio burst by ~ 1 s.

Comparing the SGR-like X-ray bursts of SGR J1935+2154 and 1E 1547.0–5408, as detected by KW data, both were in line, in terms of energy and duration, with what is usually observed from their respective sources. The spectrum, in the case of SGR J1935+2154, was harder than in typical bursts from that source and was indeed among the top 2% hardest magnetar bursts ever detected by KW (Ridnaia et al. 2020). On the other hand, the softer spectrum of 1E 1547.0–5408's burst was very typical within the magnetar population.

No further simultaneous X-ray and radio bursts were detected despite the continued X-ray activity of SGR J1935 +2154, while several fainter radio bursts were reported (Kirsten et al. 2020; Zhang et al. 2020). It is interesting to note that the latter burst's time distribution is peaked at about ± 0.2 in phase from the peak of the X-ray modulation, similar to what we observed in 1E 1547.0-5408 (Younes et al., 2020). The source entered a new radio active phase in early 2020 October, characterized by one bright burst of fluence ~ 900 Jy ms observed by CHIME, followed by many fainter bursts below 50 Jy ms observed by both CHIME and FAST (Good & Chime/Frb Collaboration 2020; Pleunis & Chime/Frb Collaboration 2020; Zhu & FAST 2020). FAST pulses were aligned in phase with the detected radio pulsation of the source.

The energy released in the brightest radio bursts of SGR J1935+2154 and 1E 1547.0–5408 is 3×10^{34} erg and 8.4×10^{30} erg, with a radio-to-X-ray ratio $E_r/E_X \sim 10^{-5}$ and $\sim 10^{-9}$, respectively. In both cases these were brighter than standard magnetar radio single peaks (below a few Jy; e.g., Camilo et al. 2006), yet "mild" compared to FRBs, although the latter are known to span a wide range of energies (Bochenek et al. 2020; The CHIME/FRB Collaboration et al. 2020). For the giant flare of SGR 1806–20 (Palmer et al. 2005) the most stringent limits to the ratio of radio versus X-ray emitted energy were set down to $\lesssim 10^{-8}$ (Tendulkar et al. 2016). On the other hand, in the case of the better constrained FRB repeaters with simultaneous X/radio observations (Scholz et al. 2017; Pilia et al. 2020) these limits are of the order of $\geqslant 10^{-9}$–10^{-8}. According to Chen et al. (2020), who derive constraints on E_r/E_X in FRBs from past surveys, E_r should be of order $\sim 10^{-5} E_X$, larger than our detection for 1E 1547.0–5408.

The wide range in radio efficiency and/or luminosity of magnetar bursts suggests that these sources may bridge the gap between "ordinary" pulsar radio bursts and the extragalactic

FRB phenomenon (as also suggested in Bochenek et al. 2020; Kirsten et al. 2020; The CHIME/FRB Collaboration et al. 2020). The detection of energetic radio bursts simultaneous with regular X-ray bursts is indicative of what has already been pointed out by previous studies (Cunningham et al. 2019; Casentini et al. 2020; Guidorzi et al. 2020; Scholz et al. 2020), i.e., that nondetections of high-energy emission from FRBs can be attributed to limiting telescopes' sensitivities rather than intrinsic inhibition of the phenomenon.

The bursts reported in this work appear to be magnetospheric in origin, given their relatively good phase alignment with the rotation of the magnetar. Lyutikov & Popov (2020) propose that magnetospheric reconnection events can explain the energetics and the apparent simultaneity of the X-ray and radio bursts of SGR J1935+2154. In the case of 1E 1547.0–5408, however, the total energy in the radio burst may still be consistent with rotation-powered emission, given its ~0.5 s duration and the estimated spin-down luminosity of the source, ~10^{35} erg s^{-1}. (Rea et al. 2012; Lyutikov et al. 2016; Esposito et al. 2020).

On the other hand, according to Lu et al. (2020), an explosion at the surface of the neutron star would produce both the X-ray burst and the radio burst, by propagating through the crust toward the polar cap in the form of Alfvén waves. In this scenario the emission is magnetospheric and it arises naturally that not all X-ray bursts generate an FRB-like radio burst, as is observed for both SGR J1935+2154 (Borghese et al. 2020) and 1E 1547.0–5408. However, the radio emission is expected to lag the X-ray burst, albeit slightly, contrary to the observations in 1E 1547.0–5408.

Moreover, both this and the external models (Margalit et al. 2020) require a ratio $L_r/L_X > 10^{-5}$–10^{-4}, which is in tension with our findings and with observations of the SGR 1806-20 giant flare.
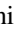
The picture emerging from our detection of radio and X-ray bursts from 1E 1547.0–5408, as well as from the most recently observed bright and faint radio and X-ray bursts from SGR J1935+2154 (Bochenek et al. 2020; Kirsten et al. 2020; The CHIME/FRB Collaboration et al. 2020; Zhang et al. 2020), is that there exists a continuum of magnetar radio burst energies, which might at times look like FRBs and at others be much closer to typical radio pulsar single pulse phenomenology (such as Rotating Radio Transients or Giant Pulses, McLaughlin et al. 2004; Lyutikov & Popov 2020). On the other hand, the X-ray counterparts of such radio bursts are not yet easily predictable, and may depend on specific parameters of the burst, most of which are still not fully understood.

Facilities: XMM-Newton, Parkes, Chandra, Swift, Konus-Wind.

Software: FTOOLS (Blackburn 1995), XSPEC (Arnaud 1996), XMM-SAS (Gabriel et al. 2004).

ORCID iDs

G. L. Israel ● https://orcid.org/0000-0001-5480-6438
M. Burgay ● https://orcid.org/0000-0002-8265-4344
N. Rea ● https://orcid.org/0000-0003-2177-6388
P. Esposito ● https://orcid.org/0000-0003-4849-5092
A. Possenti ● https://orcid.org/0000-0001-5902-3731
L. Stella ● https://orcid.org/0000-0002-0018-1687
M. Pilia ● https://orcid.org/0000-0001-7397-8091
A. Tiengo ● https://orcid.org/0000-0002-6038-1090
A. Ridnaia ● https://orcid.org/0000-0001-9477-5437
A. Y. Lien ● https://orcid.org/0000-0002-7851-9756
D. D. Frederiks ● https://orcid.org/0000-0002-1153-6340
F. Bernardini ● https://orcid.org/0000-0001-5326-2010

References

Aptekar, R. L., Frederiks, D. D., Golenetskii, S. V., et al. 1995, SSRv, 71, 265
Archibald, R. F., Kaspi, V. M., Tendulkar, S. P., & Scholz, P. 2016, ApJL, 829, L21
Arnaud, K. A. 1996, in ASP Conf. Ser. 101, Astronomical Data Analysis Software and Systems V, ed. G. H. Jacoby & J. Barnes (San Francisco, CA: ASP), 17
Beloborodov, A. M. 2017, ApJL, 843, L26
Bernardini, F., Israel, G. L., Stella, L., et al. 2011, A&A, 529, A19
Blackburn, J. K. 1995, in ASP Conf. Ser. 77, Astronomical Data Analysis Software and Systems IV, ed. R. A. Shaw, H. E. Payne, & J. J. E. Hayes (San Francisco, CA: ASP), 367
Bochenek, C. D., Ravi, V., Belov, K. V., et al. 2020, Natur, 587, 59
Borghese, A., Coti Zelati, F., Rea, N., et al. 2020, ApJL, 902, L2
Burgay, M., Israel, G. L., Possenti, A., et al. 2009, ATel, 1913, 1
Camilo, F., Cognard, I., Ransom, S. M., et al. 2007a, ApJ, 663, 497
Camilo, F., Ransom, S. M., Halpern, J. P., et al. 2006, Natur, 442, 892
Camilo, F., Ransom, S. M., Halpern, J. P., & Reynolds, J. 2007b, ApJL, 666, 93
Casentini, C., Verrecchia, F., Tavani, M., et al. 2020, ApJL, 890, L32
Chen, G., Ravi, V., & Lu, W. 2020, ApJ, 897, 146
Coti Zelati, F., Borghese, A., Rea, N., et al. 2020, A&A, 633, A31
Cunningham, V., Cenko, S. B., Burns, E., et al. 2019, ApJ, 879, 40
Dib, R., Kaspi, V. M., Scholz, P., & Gavriil, F. P. 2012, ApJ, 748, 3
Esposito, P., Rea, N., Borghese, A., et al. 2020, ApJL, 896, L30
Esposito, P., Rea, N., & Israel, G. L. 2021, in Astrophysics and Space Science Library, Vol. 461, Timing Neutron Stars: Pulsations, Oscillations and Explosions, ed. T. Belloni, M. Mendez, & C. Zhang (Berlin: Springer), 97
Gabriel, C., Denby, M., Fyfe, D. J., et al. 2004, in ASP Conf. Proc. 314, Astronomical Data Analysis Software and Systems (ADASS) XIII, ed. F. Ochsenbein, M. G. Allen, & D. Egret (San Francisco, CA: ASP), 759
Gavriil, F. P., Gonzalez, M. E., Gotthelf, E. V., et al. 2008, Sci, 319, 1802
Gehrels, N., Chincarini, G., Giommi, P., et al. 2004, ApJ, 611, 1005
Gelfand, J. D., & Gaensler, B. M. 2007, ApJ, 667, 1111
Good, D. & Chime/Frb Collaboration 2020, ATel, 14074, 1
Guidorzi, C., Marongiu, M., Martone, R., et al. 2020, A&A, 637, A69
Halpern, J. P., Gotthelf, E. V., Becker, R. H., Helfand, D. J., & White, R. L. 2005, ApJL, 632, L29
Halpern, J. P., Gotthelf, E. V., Reynolds, J., Ransom, S. M., & Camilo, F. 2008, ApJ, 676, 1178
Hobbs, G. B., Edwards, R. T., & Manchester, R. N. 2006, MNRAS, 369, 655
Israel, G. L., Esposito, P., Rea, N., et al. 2010, MNRAS, 408, 1387
Kaspi, V. M., & Beloborodov, A. M. 2017, ARA&A, 55, 261
Kirsten, F., Snelders, M., Jenkins, M., et al. 2020, NatAs, doi:10.1038/s41550-020-01246-3
Kramer, M., Stappers, B. W., Jessner, A., Lyne, A. G., & Jordan, C. A. 2007, MNRAS, 377, 107
Lamb, R. C., & Markert, T. H. 1981, ApJ, 244, 94
Li, C. K., Lin, L., Xiong, S. L., et al. 2020, arXiv:2005.11071
Lu, W., Kumar, P., & Zhang, B. 2020, MNRAS, 498, 1397
Lyutikov, M., Burzawa, L., & Popov, S. B. 2016, MNRAS, 462, 941
Lyutikov, M., & Popov, S. 2020, arXiv:2005.05093
Margalit, B., Beniamini, P., Sridhar, N., & Metzger, B. D. 2020, ApJL, 899, L27
McLaughlin, M. A., Camilo, F., Burgay, M., et al. 2004, ApJL, 605, L41
Mereghetti, S., Savchenko, V., Ferrigno, C., et al. 2020, ApJL, 898, L29
Metzger, B. D., Berger, E., & Margalit, B. 2017, ApJ, 841, 14

Palmer, D. M., Barthelmy, S., Gehrels, N., et al. 2005, Natur, 434, 1107
Pilia, M., Burgay, M., Possenti, A., et al. 2020, ApJL, 896, L40
Pintore, F., Mereghetti, S., Tiengo, A., et al. 2017, MNRAS, 467, 3467
Pleunis, Z. & Chime/Frb Collaboration 2020, ATel, 14080, 1
Rea, N., Esposito, P., Turolla, R., et al. 2010, Sci, 330, 944
Rea, N., Israel, G. L., Pons, J. A., et al. 2013, ApJ, 770, 65
Rea, N., Pons, J. A., Torres, D. F., & Turolla, R. 2012, ApJL, 748, L12
Ridnaia, A., Svinkin, D., Frederiks, D., et al. 2020, arXiv:2005.11178
Scholz, P., Camilo, F., Sarkissian, J., et al. 2017, ApJ, 841, 126
Scholz, P., Cook, A., Cruces, M., et al. 2020, ApJ, 901, 165
Scholz, P., & Kaspi, V. M. 2011, ApJ, 739, 94

Spitler, L. G., Cordes, J. M., Hessels, J. W. T., et al. 2014, ApJ, 790, 101
Spitler, L. G., Scholz, P., Hessels, J. W. T., et al. 2016, Natur, 531, 202
Tavani, M., Casentini, C., Ursi, A., et al. 2020, arXiv:2005.12164
Tendulkar, S. P., Kaspi, V. M., & Patel, C. 2016, ApJ, 827, 59
The CHIME/FRB Collaboration, Andersen, B. C., Bandura, K. M., et al. 2020,
    Natur, 587, 54
Tiengo, A., Vianello, G., Esposito, P., et al. 2010, ApJ, 710, 227
van Straten, W., Demorest, P., & Oslowski, S. 2012, AR&T, 9, 237
Younes, G., Güver, T., & Kouveliotou, C. 2020, ApJL, 904, L21
Zhang, C. F., Jiang, J. C., Men, Y. P., et al. 2020, ATel, 13699, 1
Zhu, W., Wang, B., & Zhou, D. 2020, ATel, 14084, 1